

# Separation of Negatively Charged TiO<sub>2</sub>-coated Polystyrene Beads in Microfluidic Device

Chalinee Phiphatanaphiphop,<sup>1</sup> Komgrit Leksakul,<sup>1\*</sup>

Rungrueang Phatthanakun,<sup>2</sup> Wutthikrai Busayaporn,<sup>2</sup> Chatree Saiyasombat,<sup>2</sup> Pat Phothongkam,<sup>2</sup> Isa Anshori,<sup>3</sup> MdMohosin Rana,<sup>3</sup> Hiroaki Suzuki,<sup>3</sup>

<sup>1</sup>Graduate Program in Industrial Engineering, Department of Industrial Engineering, Faculty of Engineering, Chiang Mai University, Thailand 50200

<sup>2</sup>Synchrotron Light Research Institute (Public Organization), 111 University Avenue Nakhon Ratchasima, Thailand 30000

<sup>3</sup>Graduate School of Pure and Applied Sciences, University of Tsukuba, 1-1-1 Tennodai, Tsukuba, Ibaraki, 305-8573, Japan

Corresponding author \*: E-mail address: komgrit@eng.cmu.ac.th

## Abstract

Of late, there has been much progress in assisted reproductive technology (ART) which is used to achieve pregnancy. ART is used not only to obtain higher rates of pregnancy but also for reducing communicable diseases, solving genetic disorders, and, even, sex selection. To improve ART beyond some limitations, microfluidic systems have been introduced as bio-sensing devices. As reported in the previous work, sperms with the different chromosomes X and Y have different electrical charges. Therefore, a specially designed microfluidic device with microelectrodes was fabricated to sort the different electrically charged particles. In order to examine the device, TiO<sub>2</sub>-coated polystyrene beads (TiO<sub>2</sub>-coated Ps-beads) were synthesized. The processes that are employed to fabricate and characterize the beads, such as X-ray diffraction (XRD), Tungsten Scanning Electron Microscopy (W-SEM) with energy-dispersive X-ray spectroscopy (EDS) mode, and X-ray Absorption Spectroscopy (XAS), have been reported in this work. Results show that TiO<sub>2</sub> was partly coated on the Ps-beads in the mixed form of amorphous Ti<sup>4+</sup> and had caused a negative charge to appear on the surface after fabrication and had sustained the charge for long. The beads were tested using a microfluidic device installed with microelectrodes, and it was found that the device could successfully separate the negatively charged particles from the neutral ones.

Keywords: microfluidic, microelectrodes, negatively charged, TiO<sub>2</sub>, assisted reproductive technology

## 1. Introduction

Assisted reproductive technology (ART) gains more importance at the present time as it assists people who have infertility issues to be successful in their attempts to have biological children. In most of the cases, the infertility concerns the problem of inability of sperms to fertilize an oocyte naturally [1]. Intracytoplasmic sperm injection (ICSI) and traditional *in vitro* fertilization (IVF) were introduced as

solutions to this problem. However, ICSI and IVF are not applicable in cases of low sperm count, low sperm motility, or cryopreserved samples of sperm with reduced motility [2-4]. Furthermore, the success of these techniques is highly subjective and dependent on the skill of the embryologist. To improve the rate of success, microfluidic systems have been proposed as bio-sensing devices for sorting, manipulation, detection, and characterization of sperms [5-9]. With regard to sorting of sperms for sexual selection in fertilization, [10] reported evidence of slight difference in the electrical charge between sperms with chromosome X and those with chromosome Y. Therefore, fabrication of microfluidic devices that are capable of sorting sperms for sexual selection becomes a significant topic [11]. In this work, fabrication of microfluidic devices installed with microelectrodes in order to make them capable of separating sperms is reported. To establish and initiate the process for device examination, negatively charged TiO<sub>2</sub>-coating was made to form on polystyrene beads (Ps-beads) and used instead of sperms. Methods to create negatively charged TiO<sub>2</sub>-coated Ps-beads are reported. After that, the beads were characterized. Finally, the microfluidic devices with microelectrodes were tested to separate the negatively charged TiO<sub>2</sub>-coated Ps-beads.

## 2. Materials and methods

### 2.1. *Fabricated TiO<sub>2</sub>-coated Ps-beads*

Polystyrene particles (Ps-beads) cat No. PP-50-10 size 5.98  $\mu\text{m}$  obtained from Spherotech Inc. were transferred into an Eppendorf tube containing ethanol solution in the ratio 100:1000  $\mu\text{l}$ . A micropipette was used to absorb 10  $\mu\text{l}$  of beads to spread throughout the glass, and the beads were left to dry for 30 min. Then, Ti was sputtered on the beads for around 15 min. After that, O<sub>2</sub> plasma was employed by using parameters such as 100 W of RF power and 30 Pa of pressure for 3 min. Finally, the beads were removed from the glass substrate with 12 ml of EtOH by sonication for 5 sec each time and transferred to the solution in the Eppendorf tube (1 ml of solution in each Eppendorf tube). After that, the tube was centrifuged for 15 sec and the supernatant was removed. Then, DI water of 1 ml was added to make a stock of TiO<sub>2</sub>-coated Ps-beads.

### 2.2. *Characterization of TiO<sub>2</sub>-coated Ps-beads*

#### 2.2.1. *XRD and SEM-EDS*

Crystalline structure and phase identification of TiO<sub>2</sub>-coated Ps-beads were examined by XRD experiment using a Rigaku SmartLab 9KW with Cu K $\alpha$  radiation ( $\lambda = 1.5406 \text{ \AA}$ ) to generate X-rays with a voltage of 40 kV and a current of 30 mA. Parallel beam mode was employed with incident slit at 1 mm width, length limit slit at 10 mm, and receiver slit at 20 mm. The XRD patterns were collected from 5° to 80° with increments of 0.02° and a scan rate of 3.0°/min. Tungsten scanning electron microscopy (W-SEM) was performed by FEI at 20 kV acceleration voltage. The W-SEM images were captured under secondary electron mode in a high vacuum environment. Note that the pictures of the surfaces have been captured

without any deposited element on the sample, which presents the electrical conductivity of the surface. Furthermore, energy-dispersive X-ray spectroscopy (EDS) mode was employed for elemental investigation of specific areas of the surface.

### 2.2.2. XAS

The oxidation state and local structure of TiO<sub>2</sub>-coated PS-beads were determined by X-ray absorption spectroscopy (XAS) at beamline BL1.1w, equipped with an Si (111) double-crystal monochromator, of the Synchrotron Light Research Institute (SLRI), Thailand. The SLRI storage ring was operated at an electron energy of 1.2 GeV with the electron beam current in the range of 140–80 mA. The spectra near the Ti K-edges were measured in the transmission mode at room temperature using Ti foil, Ti<sub>2</sub>O<sub>3</sub>, rutile-TiO<sub>2</sub>, and anatases-TiO<sub>2</sub> as references.

## 2.3. Microfluidic device fabrication

### 2.3.1. Design and simulation

The design of the structure for separating the negative beads is similar to the Y structure. The Comsol<sup>®</sup> program was applied for simulation of the electric field by mode electrostatics (ES) and lamina flow. The Comsol<sup>®</sup> program is a simulation tool in design for understanding, predicting, and designing microfluidic systems to manipulate stationary and time-dependent flow in two- and three-dimensional spaces. The structure was created by the layout editor<sup>®</sup> program with design for the different distances between the electrodes, 30  $\mu\text{m}$ , 50  $\mu\text{m}$ , 100  $\mu\text{m}$ , and 200  $\mu\text{m}$ , and the parameter setting was as presented in Table 1. Firstly, the structure finds the main factor for separate beads. Secondly, the total of the factors is set up using the Comsol<sup>®</sup> program and the simulation program unit is test run to get the optimal result for the electric field. Lastly, the response of the simulation is compared with the fabrication microfluidic chip.

**Table 1.** Different Parameters Being Run in Each Type in Comsol<sup>®</sup> Program

Type	Electrode (mm)		Microchannel (mm)		Voltage (V)	Distance between electrodes ( $\mu\text{m}$ )	Electric displacement field ( $\text{c/m}^2$ )
	Width	Height	Width	Height			
A	0.5	5	0.1	6	1	30	$2.88 \times 10^{-7}$
B	0.5	5	0.1	6	1	50	$2.33 \times 10^{-7}$
C	0.5	5	0.15	6	1	100	$3.32 \times 10^{-7}$
D	0.5	5	0.25	6	1	200	$1.02 \times 10^{-7}$

### 2.3.2. Photolithography process

The microfluidic chip integrated with the detected electrodes was fabricated by UV and soft lithography process, as can be seen in Figure 1. Cr/Pt layers were deposited on a substrate by sputtering and UV patterning to make electrode patterns on the resist, followed by lift-off to achieve the final electrodes, as shown in Figure 1 (a). The spin-coated positive photoresist (S-1818G) used the following conditions: 500 rpm using a time of 5 sec and 2000 rpm using a time of 10 sec. Then, the sample was baked in an oven for 30 min at 80°C and cooled down for 15 min. The pattern was irradiated with ultraviolet light for 40 sec on a glass substrate using mask aligner exposure. Next, the pattern was lifted off using toluene, which was warmed to 30°C in a water bath, and then the substrate was soaked for 30 sec. After that, the substrate was developed by using microposit<sup>TM</sup> MF-319 developer for 1 min. The sputtering metal film was deposited by Cr and Pt on the substrate and lifted off by immersing in acetone for 1 hr. To create the microchannel, UV exposure was performed to make the SU-8 25negative a photoresistant microstructure and it was developed to achieve the master mold for PDMS replication. The SU-8 25 was spin-coated to obtain a thick film of thickness 40 µm using the following conditions: 500 rpm using a time of 5 sec, slope of 10, and 1250 rpm using a time of 10 sec and exposure of 180 sec. Then, it was developed by using an SU-8 developer 2 times (the first use was of an SU-8 developer which was reused for 10 min and the second use was of an SU-8 developer which was new for 20 min) and IPA for 1 min. Next, the PDMS replicate was marked by a PDMS precursor (KE-1300T) of weight 15 g and a PDMS curing agent (CAT1300) of about 1.5 g, which were mixed in a plastic cup. A vacuum pump was used to remove the air bubbles in the PDMS solution. SU-8 irregularities poured assembling the frame for forming PDMS. As for the precursor solution SU-8 PDMS, removal of air bubbles was carried out using a vacuum pump about 2–3 times. Then, it was baked for 30 min at 80°C and left undisturbed all day. Finally, a replicated PDMS substrate which has microchannel patterns underneath covered the Cr/Pt electrode. The microfluidic chip was connected to a potentiostat to apply the potential during the time of the TiO<sub>2</sub>-negative beads flowing and passing through the electric field area between the two electrodes.

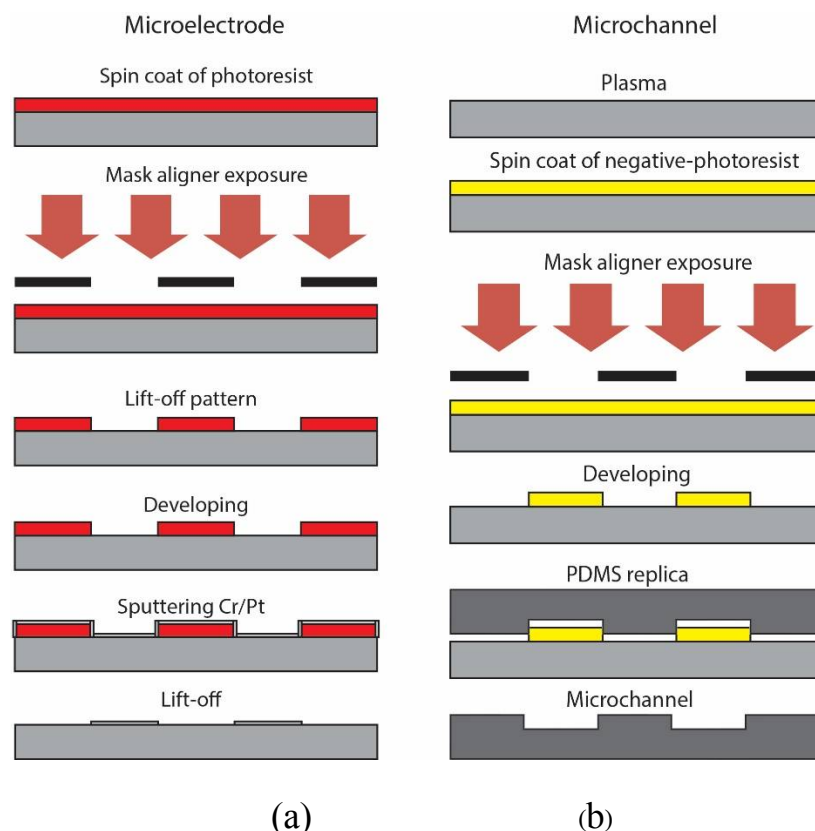


**Figure 1.** An illustration of the process of fabrication by UV and soft lithography process. (a) The microelectrode procedure and (b) the microchannel procedure.

### 3. Result and Discussion

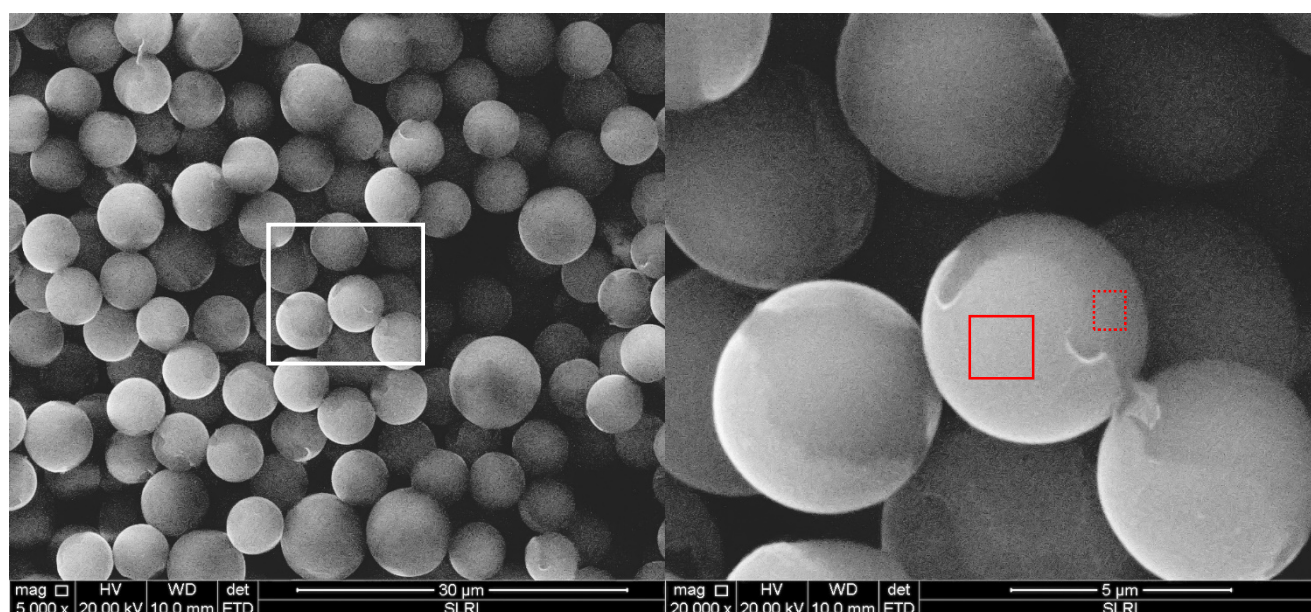
#### 3.1. $\text{TiO}_2$ -coated Ps-beads

##### 3.1.1. XRD and SEM-EDS

As for the XRD experiment, none of the crystalline peaks of  $\text{TiO}_2$  which were detected clearly expressed the amorphous form of the  $\text{TiO}_2$  structure. Therefore, the result will not be shown here. The morphology of the  $\text{TiO}_2$ -coated Ps-beads was investigated; Figure 2 (a) and Figure 2 (b) show the SEM images of the  $\text{TiO}_2$ -coated Ps-beads. In Figure 2 (a), the Ps-beads appear mostly of the same size, around 5  $\mu\text{m}$  in diameter. Note that at some ratios, the Ps-beads show the size to be slightly larger. Most of the Ps-beads exhibit incomplete surface coating as they are partly shelled. Figure 2 (b) shows the area as labeled in white rectangular shape; Figure 2 (a) is at higher magnitudes and clearly emphasizes the coating in part of the element on the surface of the Ps-beads. Moreover, elemental analysis was employed for investigation using SEM-EDS in the red rectangle areas seen in

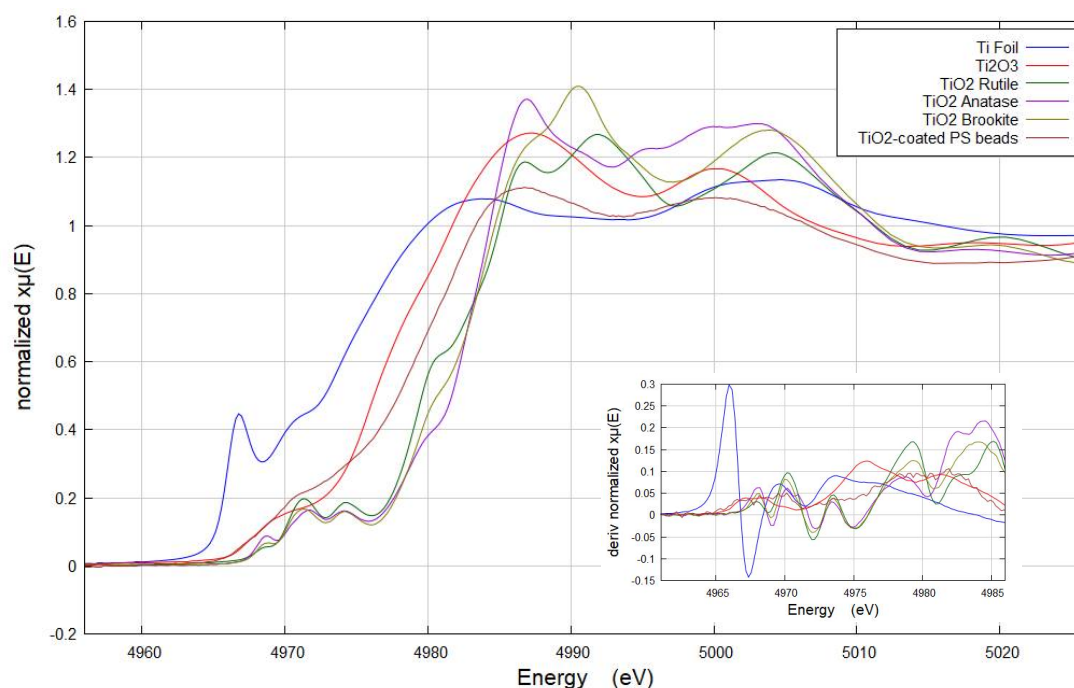


Figure 2 (b). The results reveal the spectra of Ti and O in the area labeled as a solid red rectangle. In the dotted red rectangle area, there is no sign of Ti.



**Figure 2.** (a) The SEM image of TiO<sub>2</sub>-coated Ps-beads at 5000× of magnitude. (b) 20000× magnitude of area labeled by the white rectangle in (a). SEM-EDS was used for elemental analysis for investigation of areas labeled using solid red and dotted red rectangles.

### 3.1.2. XAS



**Figure 4.** The Ti K-edge XANES experimental spectra of TiO<sub>2</sub>-coated PS-beads in comparison to the references.

The XAS spectra of TiO<sub>2</sub>-coated Ps-beads has absorption edge at 4979 eV which matches with the absorption edge of anatase-TiO<sub>2</sub> and rutile-TiO<sub>2</sub>. Therefore, the oxidation number of the TiO<sub>2</sub>-coated Ps beads clearly is Ti<sup>4+</sup>. The pre-edge feature at around 4970 eV is bound-state transition, such as the 1s → 3d transition [12]. The pre-edge of TiO<sub>2</sub>-coated Ps-beads is located at 4971 eV with 0.21 normalized pre-edge height. The position and height of the pre-edge feature directly correspond to the six-fold coordinated Ti [12-13].

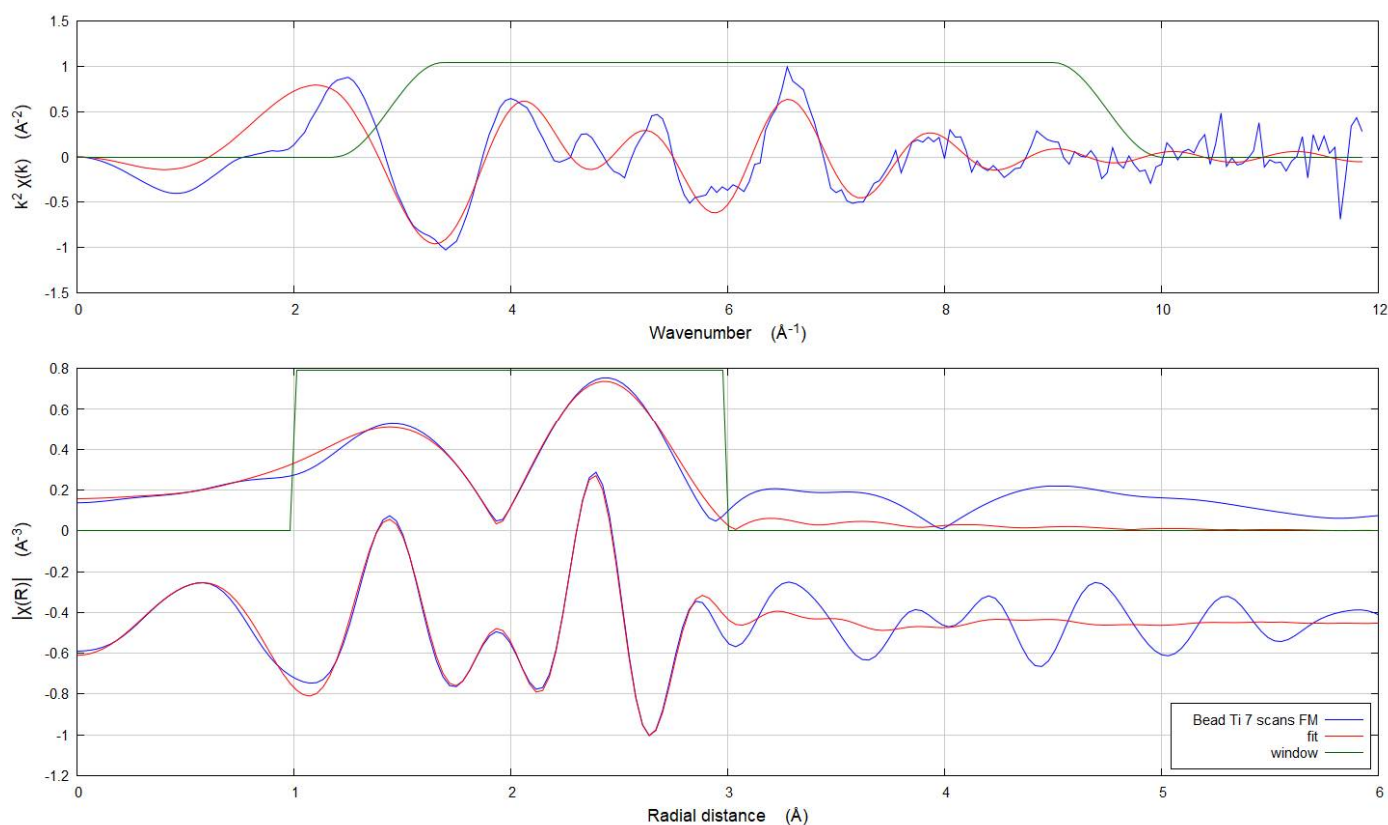


**Figure 5.** The  $k^2\chi(k)$  functions (a) and the corresponding amplitude and real part of Fourier transforms (FT) (b) of TiO<sub>2</sub>-coated Ps-beads. The red lines represent the simulations using the parameters shown in Table 2.

To find the distance from the nearest neighbor shell and the coordination number, the spectrum in energy space was transformed to  $k$  space and then transformed to  $R$  space using Fourier transform, as shown in Figure 5. In the  $R$  space without phase correction, the peaks at 1.5  $\text{\AA}$  and 2.4  $\text{\AA}$  were associated with O and Ti, respectively. EXAFS best-fit values were as reported in Table 2. The scattering amplitude ( $f_0$ ) was fixed at 0.87 which was determined from anatase-TiO<sub>2</sub>. The nearest neighbor of Ti at  $2.05 \pm 0.02$   $\text{\AA}$  was O with highly disordered Ti–O distance and had the coordination number of  $5.7 \pm 2.4$ . This coordination number

indicated that the Ti could be in the tetrahedral site and the octahedral site. However, it is more likely that Ti was in the six-fold, coordinated as evaluated from XANES. The result leads to the conclusion that the  $\text{TiO}_2$  coated on the surface was in the amorphous form and that it is mostly in the  $\text{Ti}^{4+}$  state with high surface area. This might be the factor that caused the negative charge to be able to appear on the surface for a long term.

**Table 2.** Ti K-edge EXAFS Fitted Parameters of  $\text{TiO}_2$ -coated PS-beads

Path	$N_{\text{deg}}$	$R (\text{\AA})$	$\sigma^2 (10^{-3} \text{\AA}^2)$	$E0 (\text{eV})$
Ti-O	$5.7 \pm 2.4$	$2.05 \pm 0.02$	$24 \pm 10$	$-0.04 \pm 2.00$
Ti-Ti	$1.0^a$	$2.54 \pm 0.03$	$9 \pm 1$	$-0.04 \pm 2.00$
Ti-Ti	$3.0^a$	$3.02 \pm 0.02$	$9 \pm 1$	$-0.04 \pm 2.00$

<sup>a</sup>Values without uncertainties were not determined in the fit but were held at the given value.

## 3.2. Microfluidic devices

### 3.2.1. Comsol® simulation

Simulation with the Comsol program for finding out the optimal method for the separation of the negative beads was conducted. The response values of the electric displacement field from simulation for the distances of the electrodes of 30  $\mu\text{m}$ , 50  $\mu\text{m}$ , 100  $\mu\text{m}$ , and 200  $\mu\text{m}$  were  $2.88 \times 10^{-7}$ ,  $2.33 \times 10^{-7}$ ,  $3.32 \times 10^{-7}$ , and  $1.02 \times 10^{-7} \text{ C/m}^2$ , respectively, as can be seen in Figure 6.

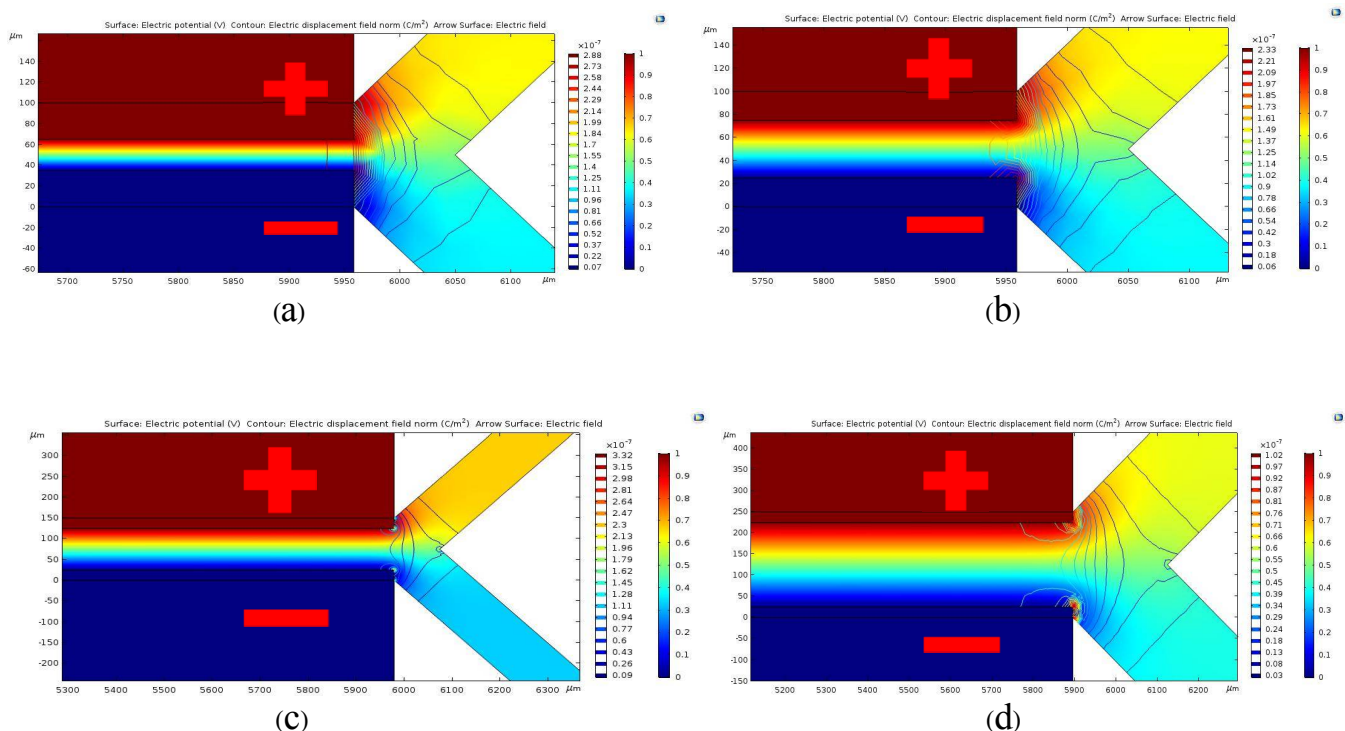


**Figure 6.** The result of the simulation by the Comsol program.



### 3.2.2. Device examination: separation of $\text{TiO}_2$ -coated Ps-beads

The microfluidic chip was fabricated by following the lithography process which has two processes, namely the electrode method and the microchannel method, as presented in Figure 7. The experiments were divided into four, based on the results of the simulation. The set-up of each of the experiments was made under a microscope and the video file was saved to observe the supporting information (S-1). When the microfluidic chip was connected to the potentiostat to apply the potential 1 Volt for 1 min, the negatively charged  $\text{TiO}_2$  was attracted by the positive electric field in the area between the two electrodes, and the negative  $\text{TiO}_2$  could be separated by following the microchannel, as demonstrated in Figure 8. The results of the running of experiments, which were repeated a total of 10 times, showed that structure C is excellent for separating negative  $\text{TiO}_2$ .

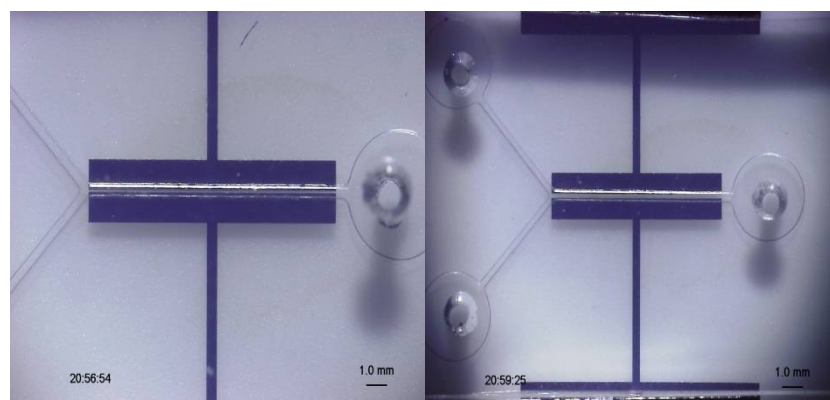


**Figure 7.** The microfluidic chip for separating negative  $\text{TiO}_2$ -beads.

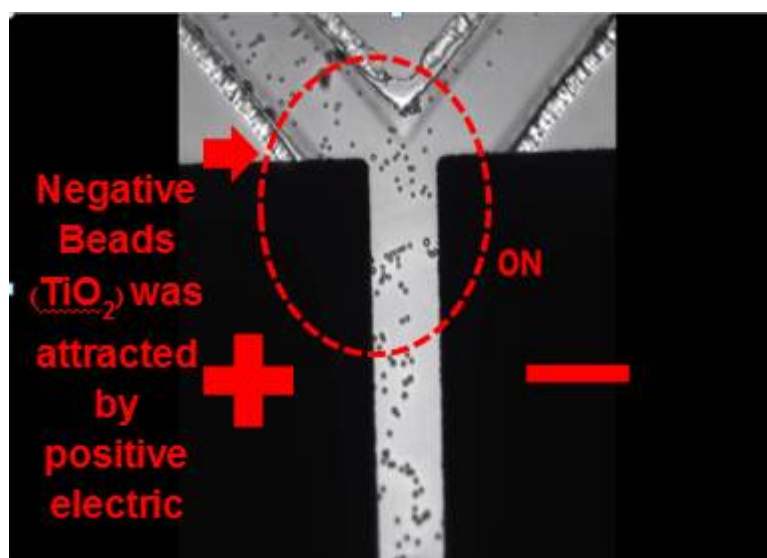


**Figure 8.** Demonstration of the negative beads being attracted by the positive electrode.

## 4. Conclusion

Negatively charged TiO<sub>2</sub>-coated Ps-beads were crafted by sputtering and O<sub>2</sub> plasma techniques. The beads were characterized using XRD, SEM-EDS, and XAS. XRD could not reveal the TiO<sub>2</sub> crystalline appearance on the beads. However, the SEM images revealed that the beads were partly coated with a thin shell of TiO<sub>2</sub>. SEM-EDS also elucidated the elemental identification of Ti and O in the coated area but not of Ti anywhere else. In the structural analysis, XAS reported the TiO<sub>2</sub> on the Ps-beads to be likely in the amorphous form of Ti<sup>4+</sup>. Combined with the result of XRD, the structure of the mixed amorphous TiO<sub>2</sub> may be the key to maintaining the negative charge on the surface of the coated Ps-beads. For the examination of the microfluidic device with microelectrodes, the device applied with 1 V for 1 min exhibited excellent capability to separate the negatively charged TiO<sub>2</sub>-coated Ps-beads. With a well-designed microchannel, the device can be successfully carried on the beads and made to induce them to different paths with the objective of sorting the different electrically charged particles.

## Acknowledgments

The Thailand Research Fund (TRF), through the Research and Researchers for Industries (RRI), PhD Program (PHD5710053), provided the financial support.

## References

- [1] Keith A, Frey MD 2010 Male reproductive health and infertility Primary Care. 37: 643.
- [2] Cooper TG, Noonan E, von Eckardstein S, Auger J, Baker HW, Behre HM, Haugen TB, Kruger T, Wang C, Mbizvo MT, Vogelsong KM 2010 World Health Organization reference values for human semen characteristics Hum. Reprod. Update. 16: 231.
- [3] Palermo G, Joris H, Devroey P, Van Steirteghem AC 1992 Pregnancies after intracytoplasmic injection of single spermatozoon into an oocyte Lancet. 340:17.
- [4] O'Connell M, McClure N, Lewis S.E.M. 2002 The effects of cryopreservation on sperm morphology, motility and mitochondrial function Hum. Reprod. 17:704.
- [5] Yan G, Wenjie L, Dimitri P 2013 Recent advances in microfluidic cell separations Analyst. 138:4714.
- [6] Yi Z, John N, Yuan W, Yu S 2013 Recent advances in microfluidic techniques for single-cell biophysical characterization Lab Chip. **13**:2464.
- [7] Niels H, Sebastian C.B, Flavio H, Andrea H 2014 Characterization of subcellular morphology of single yeast cells using high frequency microfluidic impedance cytometer Lab Chip. 14:369.

- [8] Urban S, Shady G, Robert J, Arnaud B, Philippe R 2004 Cell immersion and cell dipping in microfluidic devices *Lab Chip*. 4:148.
- [9] Ethan F, Sterling M, Jonathan Y, Saltanat N, Peter Z, Robert W 2006 Microfluidic techniques for single-cell protein expression analysis *Clin. Chem*. 52:1080.
- [10] Ute Engelmann, Franz Krassnigg, Harald Schatz, and WolfBernhard Schill, 1988 Separation of Human X and Y Spermatozoa by Free-Flow Electrophoresis, *Gamete Research* 19:151-159.
- [11] Lang Rao, Bo Cai, Jieli Wang, QianfangMeng, Chi Ma, Zhaobo He, Junhua Xu, Qinqin Huang, Shasha Li, Yi Cen, ShishangGuo, Wei Liu, and Xing-zhong Zhao, 2015 A microfluidic electrostatic separator based on pre-charged droplets, *Sensors and Actuators B* 210: 328-335
- [12] Farges, François, Gordon E. Brown Jr, and John J. Rehr. Coordination chemistry of Ti(IV) in silicate glasses and melts: I. XAFS study of titanium coordination in oxide model compounds. *Geochimica et Cosmochimicaacta* 60, no. 16 (1996): 3023-3038.
- [13] Farges, François, Gordon E. Brown, and J. J. Rehr. Ti K-edge XANES studies of Ti coordination and disorder in oxide compounds: Comparison between theory and experiment. *Physical Review B* 56, no. 4 (1997): 1809.